Schottky-quantum dot photovoltaics for efficient infrared power conversion

Keith W. Johnston, Andras G. Pattantyus-Abraham, Jason P. Clifford, Stefan H. Myrskog, Dean D. MacNeil, Larissa Levina, and Edward H. Sargent[a)]
Department of Electrical and Computer Engineering, University of Toronto, 10 King's College Rd., Toronto, Ontario M5S 3G4, Canada

(Received 8 January 2008; accepted 31 March 2008; published online 18 April 2008)

Planar Schottky photovoltaic devices were prepared from solution-processed PbS nanocrystal quantum dot films with aluminum and indium tin oxide contacts. These devices exhibited up to 4.2% infrared power conversion efficiency, which is a threefold improvement over previous results. Solar power conversion efficiency reached 1.8%. The simple, optimized architecture allows for direct implementation in multijunction photovoltaic device configurations. © *2008 American Institute of Physics*. [DOI: 10.1063/1.2912340]

Half of the sun's power reaching the earth lies in the infrared, but this power is currently underutilized in large-area, low-cost photovoltaics. Solution-processed multijunction solar cells offer the possibility of capturing each spectral band with maximal efficiency.[1] For a double junction cell, which can theoretically reach 44% efficiency under air mass 1.5 (AM1.5) illumination, the optimal bandgaps[2] correspond to 760 and 1320 nm, while a triple-junction cell can attain 50% efficiency with bandgaps corresponding to 680, 1070, and 1750 nm.

Early progress toward infrared solution-processed photovoltaics has emerged in organic materials; however, low-bandgap conjugated polymer/fullerene-derivative bulk heterojunctions remain sensitive only to 1000 nm.[3] Several other efforts have focused on sensitizing organic devices to the infrared using conjugated polymers/nanocrystal composites,[4,5] but efficiencies are still well below the best organic bulk-heterojunction devices.[6] Recent results have shown that it is possible to make efficient photovoltaic devices composed only of nanocrystals films, with response to 800 nm.[7]

By virtue of the quantum size effect, PbS colloidal quantum dots have tunable absorption characteristics that can be modified throughout the infrared spectral regime.[8] These have been used in solution-processed infrared (>1000 nm) photovoltaic devices, which had a bulk heterojunction between a conjugated polymer and PbS colloidal quantum dots.[5] It was shown in 2007 that, with the aid of a nanoporous electrode requiring high-temperature sintering and multiple cross-linking procedures, an infrared power conversion efficiency of 1.3% could be achieved.[9] However, this structure cannot be integrated with other soft materials due to the high temperatures and chemical procedures required in the device processing.

We report here simple planar, stackable PbS nanocrystal quantum dot photovoltaic devices with infrared power conversion efficiencies up to 4.2%. This represents a threefold improvement over the previous efficiencies obtained in the more complicated, stacking-incompatible nanoporous architecture.

Current-voltage characteristics of devices were measured in air. Diode lasers operating at 975 and 1550 nm were used for monochromatic illumination, while solar illumination at AM1.5 conditions was simulated with an Oriel solar simulator (Xe lamp with filters). The source intensities were measured with a Melles–Griot thermopile power meter (calibration uniform within ±5% from 300 to 2000 nm), through a 3.1 mm^2 aperture at the position of the sample. The external quantum efficiency (EQE) spectra were measured with a Keithley 6430 source-measure unit, while illumination was provided by a monochromated white light source.

Nanocrystal films were spin coated in an inert atmosphere onto indium tin oxide (ITO)-coated glass substrates from a 150 mg mL^{-1} octane solution to produce films between 100 and 300 nm thick. The Schottky contact was formed using a stack of 0.7 nm LiF/140 nm Al/190 nm Ag deposited by thermal evaporation through a shadow mask; all devices had a top contact area of 3.1 mm^2. Photocurrents were seen to scale with device area up to 7.1 mm^2, and negligible photocurrents were observed when the contacts were illuminated from the metallized side.

The device architecture is shown in Fig. 1(a). Spin coating the nanocrystals from octane solutions led to smooth, densely packed arrays, as shown by the scanning electron micrograph (SEM) in Fig. 1(a). As depicted in Fig. 1(b), a Schottky barrier was formed at the junction between thermally deposited Al and the *p*-type PbS colloidal nanocrystal film, which was recently described,[10] and was the electron-extracting contact. Photogenerated holes were extracted through the transparent conducting ITO contact.

Through optimization of the material processing steps, we dramatically improved the photovoltaic performance of this structure. The PbS nanocrystals were synthesized using an organometallic route[11] and ligand exchanged to *n*-butylamine as previously described.[12] We were able to increase device open-circuit voltage (V_{oc}) by a factor of two without lowering EQE, as shown in Fig. 2, by immediately increasing the cooling rate of the nanocrystals with an ice bath following the growth stage. This performance enhancement was attributed to improved nanocrystal passivation and hence a lower density of trap states in the semiconductor near the metal interface, which are known to affect Schottky devices.[13] To further improve the quality of the nanocrystal/Al junction, a thin LiF layer was evaporated atop the nanocrystal surface prior to Al deposition.[14]

As synthesized, the nanocrystals were passivated with ~2.5 nm long oleate ligands. These long ligands prevent close nanocrystal packing and therefore impede charge transport in films. We sought to remove as many of the long

a)Author to whom correspondence should be addressed. Electronic mail: ted.sargent@utoronto.ca.

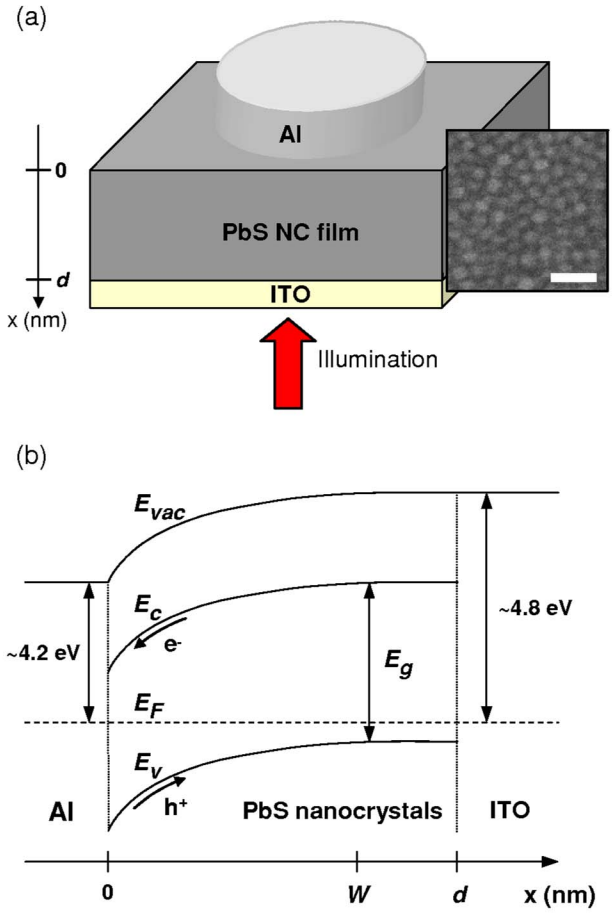

FIG. 1. (Color online) (a) Depiction of the main device architecture consisting of Al on a PbS nanocrystal (NC) film. The inset shows a SEM of the nanocrystal film (scale bar is 20 nm). (b) The energy band model, illustrating the presence of bending in the conduction band (E_c), valence band (E_v), and vacuum energy (E_{vac}) near the Al/nanocrystal interface. Photogenerated electron (e^-) and hole (h^+) transport is governed by the presence of a built-in electric field within the depletion layer (of width W) of the nanocrystal layer (of thickness d). The Fermi level (E_F) is drawn to show the p-type conduction characteristics. The bandgap (E_g) of these nanocrystals is ~0.75 eV, defined by the first maximum in the absorption spectrum.

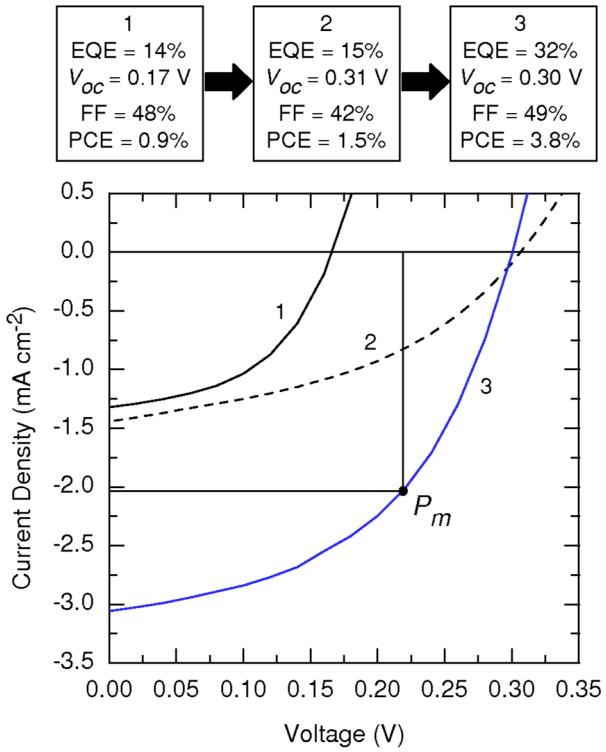

FIG. 2. (Color online) The current-voltage curve and photovoltaic performance (under 975 nm, 12 mW cm^{-2} illumination) for a device processed using the optimized passivation (dashed black, curve 2) procedure compared to the baseline (solid black, curve 1), showing an increase in V_{oc}. Nanocrystals having undergone both the optimized passivation and ligand exchange procedures (bold blue, curve 3) yielded devices with enhanced V_{oc} and EQE compared to the baseline; this is emphasized by the enclosure that represents the maximum power (P_m) load conditions. FF: fill factor and PCE: power conversion efficiency.

oleate ligands as possible and this was accomplished via repeated precipitations using methanol; a single precipitation was used for the baseline device. To fill any empty coordination sites and further displace oleate ligands from the surface, we then carried out a solution-phase ligand exchange to the ~0.6 nm long *n*-butylamine ligand. Three methanol-induced precipitations proved to be an optimal compromise between charge transport efficiency and colloidal stability. This solution-phase approach, in contrast with solid state ligand exchanges,[15] enabled the spin coating of smooth, crack-free films necessary for high-yield, large-area devices.

When coupled with the optimized passivation described above, the exchange enhancement resulted in a fourfold increase in power conversion efficiency. The photovoltaic performance of a representative device that has undergone this series of procedures appears in Fig. 2.

These optimizations allowed the fabrication of a variety of highly efficient solution-processed photovoltaic cells; those with the best performance are highlighted herein. Design A used 230 nm thick layers of PbS nanocrystals with a first excitonic transition at 1650 nm, which is close to the optimal infrared bandgap (1750 nm) in a triple-junction cell. Design B was designed for maximum power conversion at 1550 nm, using smaller nanocrystals (with enhanced absorption at this wavelength) in slightly thicker films (250 nm).

The best photovoltaic response of design A is shown in Figs. 3(a) and 3(b) under various illumination conditions. As stand-alone cells, they yielded a maximum power conversion efficiency of 1.8% under simulated solar illumination at 100 mW cm^{-2}. These devices showed up to 4.2% efficiency under monochromatic 975 nm illumination at 12 mW cm^{-2}. To demonstrate the capabilities of infrared power conversion and to simulate the conditions within multijunction cells, we filtered the simulated solar source using amorphous Si (*a*-Si) and GaAs. The *a*-Si sample transmitted wavelengths longer than 640 nm to produce an infrared intensity of 44 mW cm^{-2} incident on the device. The device converted the resultant transmitted broadband power with 1.8% efficiency. The GaAs filter transmitted 25 mW cm^{-2} at wavelengths longer than 910 nm onto the device; the measured near infrared power conversion was then 1.3%. This suggests that these photovoltaic cells could be directly stacked with other solution-processed cells to achieve efficiencies beyond the 6% mark.[6]

The best photovoltaic response of design B is shown in Fig. 3(b) under 1550 nm illumination. Monochromatic power conversion efficiencies of up to 2.1% were obtained with a 1550 nm illumination source.

A summary of the photovoltaic figures of merit obtained from the various devices is presented in Table I. While the V_{oc} values are not large in absolute terms, they are high as a

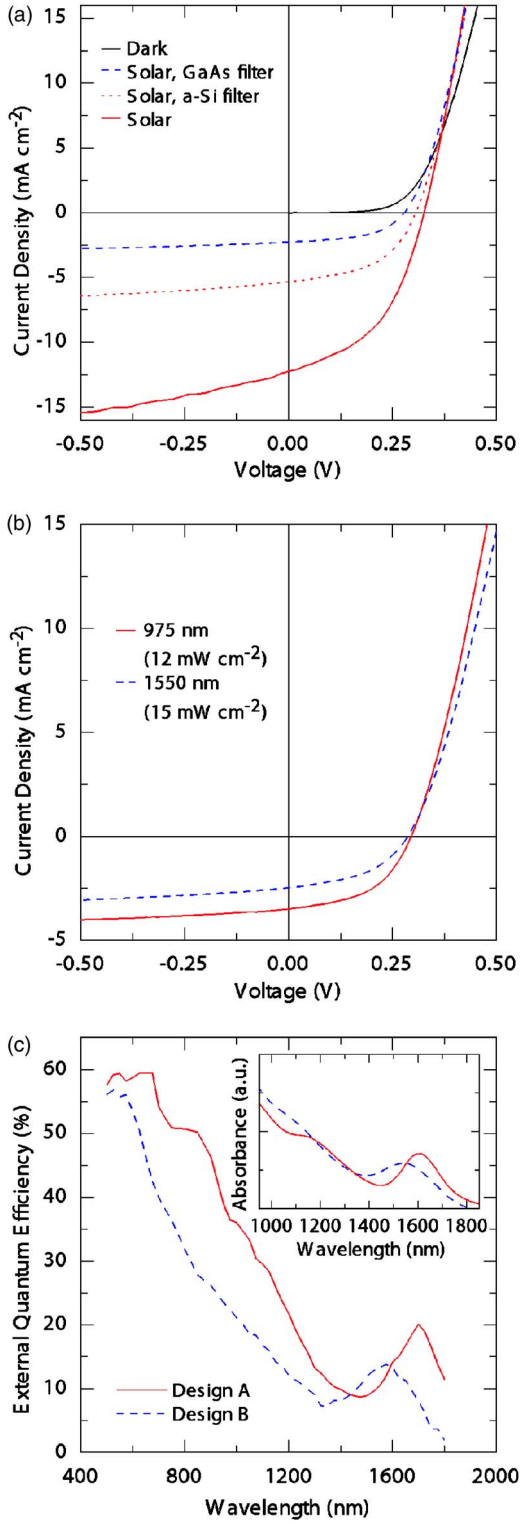

FIG. 3. (Color online) (a) Comparison of the current-voltage characteristics for design A in the dark and under illumination from variations of the simulated solar illumination source. (b) Current-voltage curves for design A (under 975 nm illumination) and design B (under 1550 nm illumination). (c) EQE spectra for designs A and B. The inset shows the absorption spectra of the ligand-exchanged nanocrystals in solution; excitonic peaks were also visible in the film absorption spectra. au: arbitrary units.

fraction of the material bandgap. Device performance was maintained for up to 5 h in air but completely degraded over 24 h. Nanocrystal films were stable in an inert environment for long durations (7 days), which indicates that encapsulation could improve long-term stability.

TABLE I. Device performance parameters; all data were obtained using design A, except under 1550 nm illumination, where design B was used. I, intensity, J_{sc}, short-circuit current density; PCE, power conversion efficiency.

Source	I (mW cm^{-2})	V_{oc} (V)	J_{sc} (mA cm^{-2})	PCE (%)
975 nm	12	0.30	3.5[a]	4.2
1550 nm	15	0.29	2.5[b]	2.1
Solar	100	0.33	12.3	1.8
Solar (*a*-Si)	44	0.31	5.4	1.8
Solar (GaAs)	25	0.28	2.3	1.3

[a]EQE 37%.
[b]EQE 13%.

We measured the EQE spectrum of devices by illuminating them with monochromatic light, measuring the current under short-circuit conditions, and scaling them with respect to the previously indicated EQEs measured at 975 and 1550 nm (for designs A and B, respectively). The EQE spectra for devices of both designs are shown in Fig. 3(c). The features of the colloidal nanocrystal absorption spectrum (inset) are manifest in the EQE spectra: a well-defined first excitonic transition is retained even in densely packed, conductive films. Film absorption data was also acquired by measuring the fraction of light reflected through the substrate and correcting for ITO and Al absorption. The film absorptions at 975 and 1550 nm were 41% and 14%, respectively, which indicate that the internal quantum efficiency exceeded 90% for the best devices. A more detailed investigation of the mechanisms leading to this efficiency has been recently published.[16]

The authors thank S. Hinds, E. Klem, G. Koleilat, G. Konstantatos, H. Shukla, and L. Soleymani for many helpful discussions and the Advanced Photovoltaics and Devices Group at the University of Toronto for the *a*-Si sample. This research was supported by the Natural Sciences and Engineering Research Council of Canada.

[1]J. Y. Kim, K. Lee, N. E. Coates, D. Moses, T. Nguyen, M. Dante, and A. J. Heeger, Science **317**, 222 (2007).
[2]A. Martí and G. L. Araújo, Sol. Energy Mater. Sol. Cells **43**, 203 (1996).
[3]M. M. Wienk, M. G. R. Turbiez, M. P. Struijk, M. Fonrodona, and R. A. J. Janssen, Appl. Phys. Lett. **88**, 153511 (2006).
[4]D. Cui, J. Xu, T. Zhu, G. Paradee, S. Ashok, and M. Gerhold, Appl. Phys. Lett. **88**, 183111 (2006).
[5]S. A. McDonald, G. Konstantatos, S. Zhang, P. W. Cyr, E. J. D. Klem, L. Levina, and E. H. Sargent, Nat. Mater. **4**, 1 (2005).
[6]K. Kim, J. Liu, M. A. G. Namboothiry, and D. L. Carroll, Appl. Phys. Lett. **90**, 163511 (2007).
[7]I. Gur, N. A. Fromer, M. L. Geier, and A. P. Alivisatos, Science **310**, 462 (2005).
[8]F. Wise, Acc. Chem. Res. **33**, 773 (2000).
[9]E. J. D. Klem, D. D. MacNeil, P. W. Cyr, L. Levina, and E. H. Sargent, Appl. Phys. Lett. **90**, 183113 (2007).
[10]J. P. Clifford, K. W. Johnston, L. Levina, and E. H. Sargent, Appl. Phys. Lett. **91**, 253117 (2007).
[11]M. A. Hines and G. D. Scholes, Adv. Mater. (Weinheim, Ger.) **15**, 1844 (2003).
[12]G. Konstantatos, I. Howard, A. Fischer, S. Hoogland, J. Clifford, E. Klem, L. Levina, and E. H. Sargent, Nature (London) **442**, 180 (2006).
[13]E. H. Rhoderick and R. H. Williams, *Metal-Semiconductor Contacts* (Clarendon, Oxford, 1988).
[14]C. J. Brabec, S. E. Shaheen, C. Winder, N. S. Sariciftci, and P. Denk, Appl. Phys. Lett. **80**, 1288 (2002).
[15]D. V. Talapin and C. B. Murray, Science **310**, 86 (2005).
[16]K. W. Johnston, A. G. Pattantyus-Abraham, J. P. Clifford, S. H. Myrskog, S. Hoogland, H. Shukla, E. J. D. Klem, L. Levina, and E. H. Sargent, Appl. Phys. Lett. **92**, 122111 (2008).